Letter

Enigma of the vortex state in a strongly correlated *d*-wave superconductor

Anushree Datta,[1,*] Hitesh J. Changlani,[2,3] Kun Yang,[2,3] and Amit Ghosal[1]
[1]*Indian Institute of Science Education and Research Kolkata, Mohanpur 741246, India*
[2]*Department of Physics, Florida State University, Tallahassee, Florida 32306, USA*
[3]*National High Magnetic Field Laboratory, Tallahassee, Florida 32310, USA*

(Received 27 July 2022; revised 2 February 2023; accepted 27 March 2023; published 20 April 2023)

We show that strong electronic repulsion transforms a vortex core from a metallic type in the overdoped regime to a Mott insulator at underdoping of a strongly correlated *d*-wave superconductor. This changeover is accompanied by an accumulation of electron density at the vortex core toward local half filling in the underdoped region, which in turn facilitates the formation of the Mott-insulating core. We find that the size of vortices evolves nonmonotonically with doping. A similar nonmonotonicity of critical field H_{c2}, as extracted from superfluid stiffness, is also found. Our results explain some recent experimental puzzles of cuprate superconductors.

DOI: 10.1103/PhysRevB.107.L140505

Introduction. Topological defects, such as vortices, have drawn significant research interest ever since Kosterlitz and Thouless [1,2] established a melting mechanism mediated by them. Vortices are low-lying excitations of type-II superconductors in the presence of magnetic fields. In conventional superconductors, a magnetic field produces a periodic array of vortices [3,4] with a normal metallic core of size ξ with circulating currents around the vortex on the scale of the penetration depth λ [5]. With increasing field H, the density of vortices increases. Beyond the critical field H_{c2}, overlapping cores suppress pairing amplitude everywhere and the superconductor transitions into a metal [3]. The study of vortices in unconventional superconductors has gathered recent momentum due to several experimental puzzles [6–8].

One such mystery lies in the mapping of the local density of states (LDOS) at the vortex core in cuprate superconductors, a prototype of strongly correlated *d*-wave superconductors (dSCs). Differential conductance in cuprates (in both $YBa_2Cu_3O_{7-\delta}$ [9] and $Bi_2Sr_2CaCu_2O_{8+\delta}$ [10]) in the optimal to underdoping region shows a gap structure, while weak-coupling calculations predict a large accumulation of low-lying states in the LDOS at the vortex core for all dopings, δ [11]. Recent experiments find similar significant pileup of the low-lying states but in the overdoped regime [7]. Several theoretical attempts have been made to understand the low-doping anomalous behaviors [12–15], including the generation of subdominant competing orders at the vortex core, such as antiferromagnetic [16–18], *s*-wave pairing [19], *d*-density wave [20,21], and pair-density wave orders [22], augmented to weak-coupling descriptions. However, no consensus has yet been achieved to comprehend the anomaly [7,23]. The role of strong correlations on the vortex inhomogeneities, however, has largely evaded the field of research; see, however, [24–26]. After all, these strong electronic repulsions turn the parent undoped ($\delta = 0$) compound to an antiferromagnetic Mott insulator [27].

Taking the route of direct inclusion of strong correlations by removing any double occupancy within a fully self-consistent microscopic calculation, our main results in this Letter are as follows: (i) The underdoped *d*-wave vortex state induces charge accumulation toward local half filling at the vortex core, and thereby promotes the emergence of "Mottness." (ii) There is a changeover of the nature of the vortex core from being Mott insulating to metallic with increasing doping, which explains the tunneling spectroscopic measurements of LDOS. (iii) The size of vortices show intriguing nonmonotonic behavior. Such a nonmonotonic behavior has other fascinating implications. For example, our result of superfluid density in the presence of magnetic field indicates that the upper critical field H_{c2} shows a dome-shaped evolution with δ, in agreement with experimental findings.

Model and methods. Strongly correlated materials can be described minimally by the Hubbard model [28] with $U \gg t$. In this limit the low-energy physics is described by a *t*-*J* model [29]:

$$\mathcal{H}_{t-J} = -t \sum_{\langle ij\rangle\sigma} \mathcal{P}\left(e^{i\phi_{ij}} \hat{c}^{\dagger}_{i\sigma} \hat{c}_{j\sigma} + \text{H.c.}\right)\mathcal{P} - \sum_i \mu \hat{n}_i + J \sum_{\langle ij\rangle} \mathcal{P}\left(\mathbf{S_i} \cdot \mathbf{S_j} - \frac{\hat{n}_i \hat{n}_j}{4}\right)\mathcal{P}. \quad (1)$$

Here $\hat{c}^{\dagger}_{i\sigma}$ ($\hat{c}_{i\sigma}$) is the creation (annihilation) operator of an electron with spin σ at lattice site i in a two-dimensional square lattice; $\mathbf{S}_i$ and $\hat{n}_i$ are the spin and electron density operators, respectively; $\langle ij\rangle$ denotes nearest-neighbor bonds; t is the hopping amplitude for an electron to its nearest neighbors; μ is the chemical potential fixing the average electron density ρ; and $J = 4t^2/U$ is the superexchange interaction

*Present address: Université Paris Cité, Laboratoire Matériaux et Phénomenes Quantiques, CNRS, F-75013 Paris, France; Université Paris-Saclay, CNRS, Laboratoire de Physique des Solides, F-91405 Orsay, France.

with U being the on-site Hubbard repulsion strength. Here, $\mathcal{P}$ is the projection operator which prohibits double occupancies on each lattice site due to the strong on-site repulsive U. The orbital magnetic field is incorporated through the Peierls factor: $\phi_{ij} = \pi/\phi_0 \int_i^j \mathbf{A} \cdot d\mathbf{l}$, where $\phi_0 = hc/2e$ is the superconducting (SC) flux quantum. We consider a uniform orbital field $\mathbf{H} = H\hat{z}$ and choose to work with the Landau gauge, $\mathbf{A} = Hx\hat{y}$.

The effect of the projection operator is implemented by the Gutzwiller approximation (GA) [30], where restriction of double occupancy is removed at the expense of renormalizing the hopping and exchange parameters: $t_{ij} \to g^t_{ij} t$, $J_{ij} \to g^J_{ij} J$; here the g's are the corresponding Gutzwiller renormalization factors (GRFs) [30,31]. The GRFs, which depend on local densities n_i, are provided in the Supplemental Material (SM) [32]. Physically, the removal of double occupancy prohibits certain hopping processes across the bond $\langle ij \rangle$, and hence the average kinetic energy must reduce on that bond from a situation where double occupancies are allowed. This is incorporated by the hopping GRFs $g^t_{ij} \leqslant 1$. Similarly, the overall higher probability of sites being singly occupied enhances the exchange coupling through g^J_{ij}. The GA formalism has been verified [37,38] to agree well with variational Monte Carlo calculations [39] (where the projections are exact) for homogeneous systems. We note that we refer to the strong correlations equivalently with the removal of double occupancy in this work.

We take advantage of the perfect periodicity of our square vortex lattice[1] by solving the eigenvalue problem using a fully self-consistent Bogoliubov–de Gennes (BdG) method on a unit cell typically of size $N = 24 \times 48$ and then extending the wave function on a system made of typically 16×8 unit cells [11,17]. We present all energies in units of the hopping amplitude t and set the temperature $T = 0$ for our calculations. We use $J = 0.33$—a typical value used for cuprate superconductors [40]. We consider several doping ($\delta = 1 - \rho$) values ranging from $\delta = 0.06$ (underdoped) to $\delta = 0.25$ (overdoped). To emphasize our key findings, we compared our results from Gutzwiller inhomogeneous mean-field theory (GIMT) with results from standard inhomogeneous mean-field theory (IMT), where the effects of projection $\mathcal{P}$ are ignored by taking the Gutzwiller factors to be unity, i.e., with double occupancy being allowed. In IMT, we tune J values for each doping in such a way that both IMT and GIMT yield the same d-wave gap when the magnetic field is zero [41]. The details of GIMT and IMT calculations are included in the SM [32].

d-wave SC order. We begin describing our results by elaborating on the dSC order parameter calculated within the GIMT framework: $\langle \hat{c}_{i\sigma} \hat{c}_{j\bar{\sigma}} \rangle_\psi \approx g^t_{ij} \Delta_{ij}$ [42,43]. Here $\langle \ldots \rangle_\psi$ denotes the expectation value in the truncated Hilbert space with double occupancies removed. The spatial profile of the dSC order parameter, $\Delta_d^{\rm OP}(\mathbf{r}_i) = \frac{J}{4}|(g^t_{i,i+\hat{x}}\Delta_{i,i+\hat{x}} + g^t_{i,i-\hat{x}}\Delta_{i,i-\hat{x}} - e^{ibx} g^t_{i,i+\hat{y}}\Delta_{i,i+\hat{y}} - e^{-ibx} g^t_{i,i-\hat{y}}\Delta_{i,i-\hat{y}})|$ (here $b \equiv H/\phi_0$) is shown in Fig. 1. Different panels of Fig. 1 show $\Delta_d^{\rm OP}(\mathbf{r}_i)$ for representative δ. Away from a vortex core, i.e., near the boundary of the magnetic unit cell containing a single SC flux quantum, $\Delta_d^{\rm OP}$ attains the homogeneous Bardeen-Cooper-Schrieffer (BCS) value while it falls at the vortex core. This conical-shaped fall at the core for overdoped [Fig. 1(a)] to optimally doped [Figs. 1(b) and 1(c)] systems follows the expected $\tanh(r/\xi)$ behavior, where ξ is the SC coherence length [5]. In contrast, the fall of $\Delta_d^{\rm OP}(\mathbf{r}_i)$ shows a strikingly different pattern at underdoping [Fig. 1(d)]: The region of the depletion of $\Delta_d^{\rm OP}(\mathbf{r}_i)$ is much wider—near the core center, the vortex resembles a "flat-bottom bowl." The weak-coupling IMT calculations preserve the conical-shaped vortex for all δ, and shrink monotonically toward underdoping; see the SM [32].

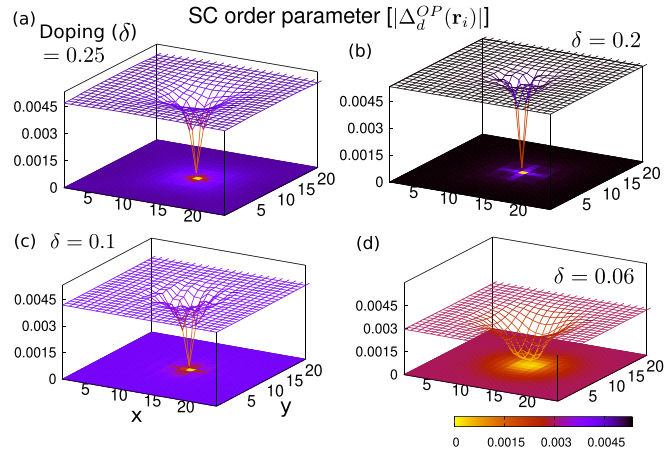

FIG. 1. SC order parameter profiles. d-wave SC $|\Delta_d^{\rm OP}(\mathbf{r}_i)|$ profiles around a vortex core on a magnetic cell of size 24×24 at different doping (δ) values. The fall of $\Delta_d^{\rm OP}(\mathbf{r}_i)$ at the vortex center has the conventional conical form at $\delta = 0.25$, 0.2, and takes up a form of a "flat-bottom bowl" at $\delta = 0.06$.

Local charge density at a vortex core. In order to develop a deeper insight into the above results we next study the local charge density near the vortex core location $\mathbf{r}_v$[2] for different δ. In the optimally doped region ($\delta = 0.2$), the spatial density profile features a weak dip around $\mathbf{r}_v$ [Fig. 2(a)], consistent with the weak-coupling theory. Upon lowering δ, the $n_{\mathbf{r}_v}$ rises rapidly to near unity by $\delta = 0.06$ [Fig. 2(c)]. This enhancement of $n_{\mathbf{r}_v}$ characterizes the emergence of "Mottness" at the vortex core region for an average doping not so close to unity. Thus, for $\delta \lesssim 0.06$ the vortex core becomes insulating and $g^t_{ij} \approx 0$ quenching the kinetic energy at the core. The effective picture of the underlying normal state in the core becomes that of an undoped patch of an (antiferromagnetic) Mott insulator,

[1] A triangular vortex lattice is energetically favorable within a continuum Ginzburg-Landau theory, which ignores underlying lattice symmetries. However, it is numerically challenging to study the triangular vortex lattice with an underlying square lattice of finite size. Also, the connection between the structure of the vortex lattice and the crystal lattice symmetry is observed experimentally in conventional s-wave superconductors [58].

[2] While $\mathbf{r}_v$ represents the center of a vortex, for a better resolution of different local observables, e.g., LDOS at the vortex core, we gather statistics not just at the vortex center but on a 2×2 lattice site around the vortex center. Thus $\mathbf{r}_v$ represents the location of the "vortex core region".

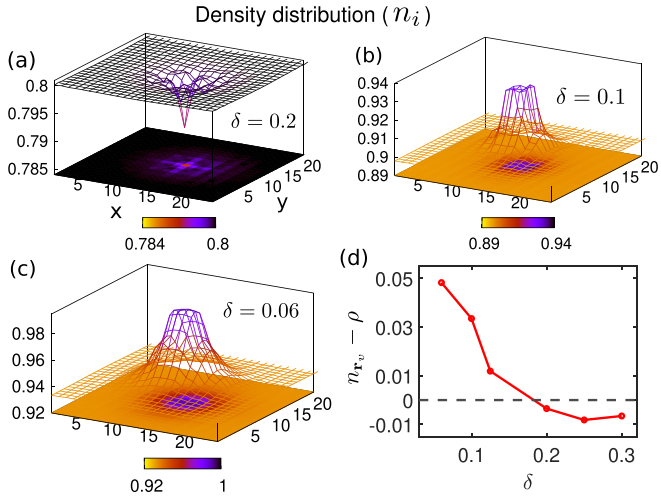

FIG. 2. Electronic charge density distribution. Local density n_i maps around a vortex core for different δ. At the vortex core, at $\delta = 0.2$ [panel (a)], n_i features a dip, and at $\delta = 0.1$, 0.06 [panels (b) and (c)], the electronic charges accumulate to form a hill (with core density approaching unity). Panel (d) shows the profile of $n_{\mathbf{r}_v} - \rho$ vs δ. The $n_{\mathbf{r}_v}$ values are less than ρ for $\delta > 0.18$ and greater than ρ for $\delta < 0.18$. At $\delta = 0.06$, $n_{\mathbf{r}_v}$ approaches unity leading to formation of a Mott-insulating core.

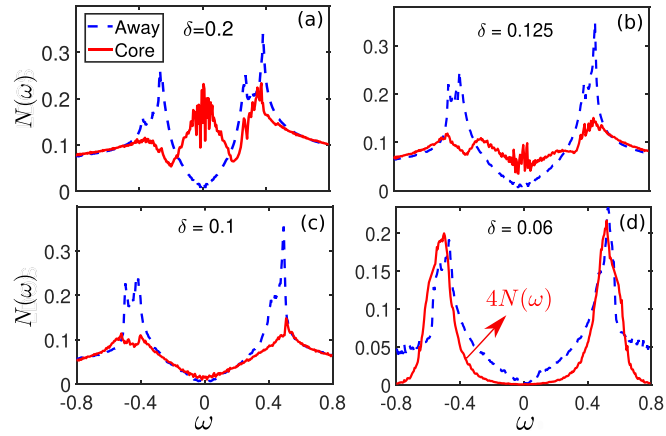

FIG. 3. Local density of states. LDOS at the vortex core (red traces) and away from the core (blue traces) for $\delta = 0.2$ (a), $\delta = 0.125$ (b), $\delta = 0.1$ (c), and $\delta = 0.06$ (d). For $\delta = 0.2$, the LDOS features a midgap peak which gradually reduces with decreasing δ. For $\delta = 0.06$, a hard gap opens with sharp peaks at $\omega \approx \pm J_{\text{eff}}/2$. In panel (d), the vortex core LDOS is scaled up by a factor of 4, for visual clarity.

described by a local Heisenberg model. This is quite unlike the Abrikosov vortex with a metallic core [5]. We note that the vortex core here is not simply serving as a window to the underlying normal state in the sense that the underlying normal state at $\delta = 0.06$ without the vortex is not yet a Mott insulator. Instead, the Mott vortex core here is a result of strong correlations and a by-product of charge accumulation due to it. However we should also emphasize that this limit of the vortex core is realized only in the proximity of the undoped Mott insulator. The reorganization of the local charge density at the vortex core as a function of doping is shown in Fig. 2(d). We find the excess local charge density at the vortex core changes sign with δ near optimal doping.

The nonlinear effects of GRFs in the effective chemical potential μ_i, obtained while minimizing the total ground state energy of the system, play a key role in driving vortex cores toward Mottness; see the SM for additional details [32]. Such effects not only drive the vortex core toward Mottness but also help the nearby sites of the vortex core to attain local half filling forming a near plateau in n_i [Fig. 2(c)]. The occurrence of a plateau in n_i in the core region is ultimately connected to the "flat-bottom bowl" structure of Δ_d^{OP}. The charge fluctuations freeze on these sites, as $t_{ij} \approx 0$, depleting dSC order over an extended region.

We emphasize that the removal of double occupancy is crucial for the aforementioned charge accumulation at the core and subsequent effects. Without the removal of double occupancy, we verified that the weak dip in n_i at the vortex core, a feature of overdoping, continues until the lowest doping; see the SM [32].

LDOS at the vortex core. The emergence of Mottness has important implications for the LDOS at the vortex core as we discuss below. In an s-wave superconductor, Andreev-like zero-energy bound states [44] were predicted theoretically to appear in the vortex cores and have also been observed experimentally in tunneling measurements [45]. For a dSC, similar accumulation of the low-energy core states (LECS) is also predicted within the IMT calculation [11], even though true bound states are not found due to the collapse of the d-wave gap along the nodal directions. Such LECS are reminiscent of the metallic nature of the vortex core. However, the differential tunneling conductance map in cuprates shows no signatures of LECS in underdoped to optimally doped samples, beyond some subgap features [9,10]. In contrast, recent experiments in overdoped samples showed prominent LECS at the vortex core [7].

To uncover this mystery, we show in Fig. 3 the LDOS with varying doping δ in GIMT. Within GIMT, the LDOS is calculated using [41,46]: $N(\mathbf{r}_i, \omega) = N_e^{-1} \sum_{k,n} g_{ii}^t [|u_n^k(\mathbf{r}_i)|^2 \delta(\omega - E_{k,n}) + |v_n^k(\mathbf{r}_i)|^2 \delta(\omega + E_{k,n})]$, where $\{u_n^k(\mathbf{r}_i), v_n^k(\mathbf{r}_i)\}$ are the local Bogoliubov wave functions, $E_{k,n}$ are corresponding energy eigenvalues (see the SM [32]), and N_e is the total number of eigenstates. As shown Fig. 3(a) the LDOS near the vortex cores is found to feature a peak near zero energy for optimal doping $\delta = 0.2$. We find a similar peak at $\omega \approx 0$ in the LDOS near the vortex core for doping $\delta > 0.2$. Thus, LECS are present in the overdoped to optimally doped region, which also agrees with the weak-coupling predictions [11]. However, the vortex core LDOS at $\delta = 0.125$ in Fig. 3(b) shows a depletion in zero-energy states and subgap features. With decreasing doping the low-energy states get further suppressed and no LECS can be seen in Fig. 3(c). Upon further lowering doping to $\delta = 0.06$, the vortex core LDOS exhibits a U-shaped (hard) gap, as depicted in Fig. 3(d). This gap can be explained by the change in the nature of the vortex core with core density approaching unity for $\delta = 0.06$ as seen in Fig. 2(c). The Mott cluster of sites at the vortex core, being described by an effective Heisenberg model as discussed already, features lowest-lying excited states beyond a spin gap $\approx J_{\text{eff}}$ [43,47]. The tantalizing similarity of our finding of LDOS with experiments is truly intriguing. In IMT

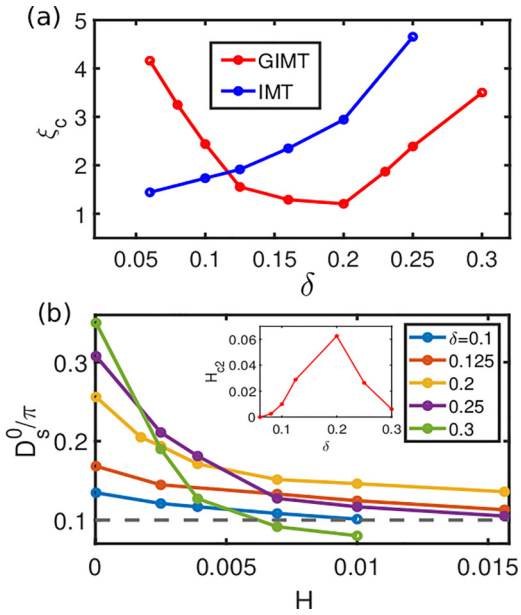

FIG. 4. Vortex core size and critical magnetic field from superfluid density. Panel (a) depicts the variation of the vortex core length scale ξ_c as a function of doping, from IMT (blue trace) and GIMT (red trace) calculations. In IMT, ξ_c shrinks monotonically with decreasing doping. In GIMT, ξ_c shows a nonmonotonic behavior. Values of ξ_c are in the unit of the lattice spacing. Panel (b) shows the variations of superfluid density D_s^0 as a function of magnetic field H at different doping values. The threshold value for estimating the critical magnetic field H_{c2} is set at $D_s^0/\pi = 0.1$, as marked by the black horizontal line. The inset in panel (b) shows the behavior of the obtained H_{c2} with respect to δ, featuring a domelike profile. The H values are represented in the unit of ϕ_0.

calculations, prominent LECS are always present at the vortex core for all δ; see the SM [32].

Nonmonotonicity in the core size. The unfolding of Mottness causes an intriguing nonmonotonic variation of the core size with δ, as we examine below.

For definiteness, we define the vortex length scale ξ_c as the distance from the vortex center where the order parameter $\Delta_d^{\rm OP}(i)$ recovers 80% of its maximum value. The red trace in Fig. 4(a), representing $\xi_c(\delta)$, captures the two trends above and below the optimal doping $\delta \approx 0.2$. For $\delta > 0.2$, ξ_c shrinks as the doping value is decreased. This is consistent with the BCS expectation, where $\xi_c \sim v_f/\pi E_{\rm gap}$, with v_f and $E_{\rm gap}$ being the Fermi velocity and the energy gap, respectively. Since $E_{\rm gap}$ increases with decreasing δ within a d-wave BCS description, the vortex core shrinks. In the region below $\delta \approx 0.2$, ξ_c ceases to follow the $v_f/\pi E_{\rm gap}$ trend and starts to increase continuously as doping is lowered toward $\delta \to 0$. As discussed earlier, in the strong underdoped limit the congregation of Mott sites makes the variation of $\Delta_d^{\rm OP}$ near the vortex core flatter. Our findings indicate that the enhancement of ξ_c in the underdoped regime is intimately connected with the formation of a Mott cluster. It is indeed fascinating that the nonmonotonicity in the vortex state tracks the non-BCS behavior [27]. A similar nonmonotonic doping dependence has been theoretically discussed also for the SC coherence length in strongly correlated superconductors [39].

To further highlight the prominent dependence of the vortex core size on strong correlations, we also include the trace of ξ_c from IMT calculations in Fig. 4(a), which shows only a monotonic increase with δ in the entire range.

Superfluid stiffness and critical magnetic field. Having encountered the nonmonotonic dependence of ξ_c with δ, we next turn our attention to superfluid stiffness D_s which gives rise to the Meissner effect [5]. Here we focus on the δ dependence of H_{c2} within the GIMT framework. In what follows, we calculate D_s using the Kubo formalism [48]: $D_s/\pi = \langle -k_x \rangle - \Lambda_{xx}(q_x = 0, q_y \to 0, \omega_n = 0)$, where $\langle -k_x \rangle$ is the average kinetic energy along the x direction and $\Lambda_{xx}(\mathbf{q}, \omega)$ is the transverse current-current correlation function. In order to obtain the $H_{c2}(\delta)$, in Fig. 4(b) we plot D_s as a function of H, at different values of δ. Because the BdG technique does not include quantum phase fluctuations of SC order, D_s is not driven to zero by the fluctuations in the dSC pairing amplitude alone (which are fully included in BdG method). However, because the BdG calculation results in a significant reduction of D_s to a low value, it is expected that quantum phase fluctuations, riding on top of the fluctuations in the pairing amplitude, would guide D_s to zero. We thus consider a small threshold value of $D_s/\pi = 0.1$ to mark off H_{c2}. Even though such extraction of H_{c2} will not be an accurate estimate of the upper critical fields, we believe it to represent the qualitative doping dependence of the *true* H_{c2}.

The behavior of the extracted critical field H_{c2} in the inset of Fig. 4(b) features a dome-shaped profile with its maximum residing at $\delta \approx 0.2$ (optimal doping). Similar nonmonotonic behavior in H_{c2} versus δ has been recently observed in cuprate superconductors [49]. Interestingly, this finding gels well with the size of the vortex core, because in Ginzburg-Landau theories, $H_{c2} = \phi_0/2\pi\xi^2$, where the coherence length ξ is the characteristic length scale of the vortex core. Thus a nonmonotonicity in the core size, as seen in Fig. 4(a), implies a nonmonotonicity in H_{c2} as well. Interestingly, in cuprates the maximum of H_{c2} occurs near the optimal doping [50,51], similar to our findings.

Conclusion. We illustrated how the nature of the vortex core changes from metallic type in the overdoped regime to a Mott-insulating one upon approaching undoping of a strongly correlated dSC. This changeover is accompanied by accumulation of the electronic charge at vortex core toward half filling, which in turn facilitate the formation of a Mott-insulating core. It will be interesting to track the charge of vortices using cavity electromechanics measurements [52]. The change of the nature of vortex explains the anomaly in the LDOS with dopings. The shape of the vortices changes as well, leading to a nonmonotonic evolution of the vortex core size, which in turn explains the experimental signatures of H_{c2}. These features stem from the non-BCS features due to the proximity to a Mott insulator. A high value of H_{c2} near optimal doping is also sometimes associated to the presence of a quantum critical point in the literature [53]. Our results do not depend on the presence of any quantum critical point near optimal doping. However, it will be an interesting future direction to connect our findings to a pos-

sible quantum critical point. Possible presence of competing orders can fine-tune the scenario by bringing in additional length scales. It should also be noted that our real-space calculations naturally produce competing superconducting orders like extended *s*-wave order. However, the amplitude of the extended *s*-wave order is extremely small and thus unlikely to have a significant effect on the LDOS. Our findings can have important implications on properties of other materials like Fe-based superconductors and twisted bilayer graphene, where strong correlation physics is believed to play a crucial role [54–57].

Acknowledgment. We thank M. Randeria for valuable comments. We acknowledge support from the Scheme of Promotion of Academic and Research collaboration (Grant No. 460). A.D. acknowledges support at Instituto de Ciencia de Materiales de Madrid, CSIC (under Grant No. PGC2018-097018-B-I00). The work of K.Y. was supported by the National Science Foundation (Grant No. DMR-1932796). The work of H.J.C. was supported by NSF-CAREER Grant No. DMR-2046570. The works of K.Y and H.J.C were performed at the National High Magnetic Field Laboratory, which is supported by National Science Foundation Cooperative Agreement No. DMR-1644779, and the State of Florida. The computations were facilitated by Dirac cluster at IISER Kolkata and Research Computing Cluster (RCC) at Florida State University.

[1] J. M. Kosterlitz and D. J. Thouless, J. Phys. C: Solid State Phys. **6**, 1181 (1973).
[2] J. M. Kosterlitz, Rev. Mod. Phys. **89**, 040501 (2017).
[3] A. Abrikosov, J. Phys. Chem. Solids **2**, 199 (1957).
[4] N. Kopnin, *Vortices in Type-II Superconductors: Structure and Dynamics* (Oxford University Press, Oxford, 2001).
[5] M. Tinkham, *Introduction to Superconductivity*, Dover Books on Physics Series (Dover Publications, New York, 2004).
[6] J.-X. Yin, Z. Wu, J.-H. Wang, Z.-Y. Ye, J. Gong, X.-Y. Hou, L. Shan, A. Li, X.-J. Liang, X.-X. Wu, J. Li, C.-S. Ting, Z.-Q. Wang, J.-P. Hu, P.-H. Hor, H. Ding, and S. H. Pan, Nat. Phys. **11**, 543 (2015).
[7] T. Gazdić, I. Maggio-Aprile, G. Gu, and C. Renner, Phys. Rev. X **11**, 031040 (2021).
[8] S. D. Edkins, A. Kostin, K. Fujita, A. P. Mackenzie, H. Eisaki, S. Uchida, S. Sachdev, M. J. Lawler, E.-A. Kim, J. C. S. Davis, and M. H. Hamidian, Science **364**, 976 (2019).
[9] I. Maggio-Aprile, C. Renner, A. Erb, E. Walker, and O. Fischer, Phys. Rev. Lett. **75**, 2754 (1995).
[10] S. H. Pan, E. W. Hudson, A. K. Gupta, K.-W. Ng, H. Eisaki, S. Uchida, and J. C. Davis, Phys. Rev. Lett. **85**, 1536 (2000).
[11] Y. Wang and A. H. MacDonald, Phys. Rev. B **52**, R3876(R) (1995).
[12] P. Nikolić, S. Sachdev, and L. Bartosch, Phys. Rev. B **74**, 144516 (2006).
[13] A. Melikyan and Z. Tešanović, Phys. Rev. B **76**, 094509 (2007).
[14] H. Tsuchiura, M. Ogata, Y. Tanaka, and S. Kashiwaya, Phys. Rev. B **68**, 012509 (2003).
[15] O. Vafek, A. Melikyan, M. Franz, and Z. Tešanović, Phys. Rev. B **63**, 134509 (2001).
[16] J.-X. Zhu and C. S. Ting, Phys. Rev. Lett. **87**, 147002 (2001).
[17] A. Ghosal, C. Kallin, and A. J. Berlinsky, Phys. Rev. B **66**, 214502 (2002).
[18] Y. Zhang, E. Demler, and S. Sachdev, Phys. Rev. B **66**, 094501 (2002).
[19] A. Himeda, M. Ogata, Y. Tanaka, and S. Kashiwaya, J. Phys. Soc. Jpn. **66**, 3367 (1997).
[20] M. M. Maśka and M. Mierzejewski, Phys. Rev. B **68**, 024513 (2003).
[21] K. Seo, H.-D. Chen, and J. Hu, Phys. Rev. B **76**, 020511(R) (2007).
[22] Z. Dai, Y.-H. Zhang, T. Senthil, and P. A. Lee, Phys. Rev. B **97**, 174511 (2018).
[23] J. Bruér, I. Maggio-Aprile, N. Jenkins, Z. Ristić, A. Erb, C. Berthod, Ø. Fischer, and C. Renner, Nat. Commun. **7**, 11139 (2016).
[24] L. B. Ioffe and A. J. Millis, Phys. Rev. B **66**, 094513 (2002).
[25] Q.-H. Wang, J. H. Han, and D.-H. Lee, Phys. Rev. Lett. **87**, 167004 (2001).
[26] J. H. Han and D.-H. Lee, Phys. Rev. Lett. **85**, 1100 (2000).
[27] P. A. Lee, N. Nagaosa, and X.-G. Wen, Rev. Mod. Phys. **78**, 17 (2006).
[28] D. Scalapino, Phys. Rep. **250**, 329 (1995).
[29] P. W. Anderson, P. A. Lee, M. Randeria, T. M. Rice, N. Trivedi, and F. C. Zhang, J. Phys.: Condens. Matter **16**, R755 (2004).
[30] W.-H. Ko, C. P. Nave, and P. A. Lee, Phys. Rev. B **76**, 245113 (2007).
[31] F. C. Zhang, C. Gros, T. M. Rice, and H. Shiba, Supercond. Sci. Technol. **1**, 36 (1988).
[32] See Supplemental Material at http://link.aps.org/supplemental/10.1103/PhysRevB.107.L140505 for details on GRFs, GRF augmented inhomogeneous mean-field theory calculations, order parameter and local density of states from the standard inhomogeneous mean-field theory, and role of the GRFs on emerging Mottness at vortex cores; the material includes Refs. [33–36].
[33] K.-Y. Yang, W. Q. Chen, T. M. Rice, M. Sigrist, and F.-C. Zhang, New J. Phys. **11**, 055053 (2009).
[34] R. B. Christensen, P. J. Hirschfeld, and B. M. Andersen, Phys. Rev. B **84**, 184511 (2011).
[35] D. I. Khomskii and A. Freimuth, Phys. Rev. Lett. **75**, 1384 (1995).
[36] G. Blatter, M. Feigel'man, V. Geshkenbein, A. Larkin and A. van Otterlo, Phys. Rev. Lett. **77**, 566 (1996).
[37] R. Sensarma, M. Randeria, and N. Trivedi, Phys. Rev. Lett. **98**, 027004 (2007).
[38] A. Himeda and M. Ogata, Phys. Rev. B **60**, R9935(R) (1999).
[39] A. Paramekanti, M. Randeria, and N. Trivedi, Phys. Rev. Lett. **87**, 217002 (2001).
[40] M. R. Norman, M. Randeria, H. Ding, and J. C. Campuzano, Phys. Rev. B **52**, 615 (1995).
[41] A. Garg, M. Randeria, and N. Trivedi, Nat. Phys. **4**, 762 (2008).
[42] N. Fukushima, Phys. Rev. B **78**, 115105 (2008).
[43] D. Chakraborty, R. Sensarma, and A. Ghosal, Phys. Rev. B **95**, 014516 (2017).

[44] C. Caroli, P. D. Gennes, and J. Matricon, Phys. Lett. **9**, 307 (1964).
[45] M. Chen, X. Chen, H. Yang, Z. Du, X. Zhu, E. Wang, and H.-H. Wen, Nat. Commun. **9**, 970 (2018).
[46] A. Datta, K. Yang, and A. Ghosal, Phys. Rev. B **100**, 035114 (2019).
[47] P. W. Anderson, Phys. Rev. Lett. **96**, 017001 (2006).
[48] D. J. Scalapino, S. R. White, and S. Zhang, Phys. Rev. B **47**, 7995 (1993).
[49] H. H. Wen, H. P. Yang, S. L. Li, X. H. Zeng, A. A. Soukiassian, W. D. Si, and X. X. Xi, Europhys. Lett. **64**, 790 (2003).
[50] B. J. Ramshaw, J. Day, B. Vignolle, D. LeBoeuf, P. Dosanjh, C. Proust, L. Taillefer, R. Liang, W. N. Hardy, and D. A. Bonn, Phys. Rev. B **86**, 174501 (2012).
[51] Y. Wang and H.-H. Wen, Europhys. Lett. **81**, 57007 (2008).
[52] S. K. Sahu, S. Mandal, S. Ghosh, M. M. Deshmukh, and V. Singh, Nano Lett. **22**, 1665 (2022).
[53] G. Grissonnanche, O. Cyr-Choinière, F. Laliberté, S. René de Cotret, S. Juneau-Fecteau, S. Dufour-Beauséjour, M.-È Delage, D. LeBoeuf, J. Chang, B. J. Ramshaw, D. A. Bonn, W. N. Hardy, R. Liang, S. Adachi, N. E. Hussey, B. Vignolle, C. Proust, M. Sutherland, J.-H. Park, D. Graf, N. Doiron-Leyraud *et al.*, Nat. Commun. **5**, 3280 (2014).
[54] P. O. Sprau, A. Kostin, A. Kreisel, A. E. Böhmer, V. Taufour, P. C. Canfield, S. Mukherjee, P. J. Hirschfeld, B. M. Andersen, and J. C. S. Davis, Science **357**, 75 (2017).
[55] L. de' Medici, G. Giovannetti, and M. Capone, Phys. Rev. Lett. **112**, 177001 (2014).
[56] D. Wang, L. Kong, P. Fan, H. Chen, S. Zhu, W. Liu, L. Cao, Y. Sun, S. Du, J. Schneeloch, R. Zhong, G. Gu, L. Fu, H. Ding, and H.-J. Gao, Science **362**, 333 (2018).
[57] Y. Cao, V. Fatemi, A. Demir, S. Fang, S. L. Tomarken, J. Y. Luo, J. D. Sanchez-Yamagishi, K. Watanabe, T. Taniguchi, E. Kaxiras, R. C. Ashoori, and P. Jarillo-Herrero, Nature (London) **556**, 80 (2018).
[58] S. C. Ganguli, H. Singh, R. Ganguly, V. Bagwe, A. Thamizhavel, and P. Raychaudhuri, J. Phys.: Condens. Matter **28**, 165701 (2016).